Energy Storage Emulation in Islanded Low Voltage Grid

Nora Plassbak Sagatun
Department of Electric Power Engineering
Norwegian University of Science and Technology
Trondheim, Norway
nora.sagatun@gmail.com

Santiago Sanchez
Department of Electric Power Engineering
Norwegian University of Science and Technology
Trondheim, Norway
santiags@ntnu.no

Elisabetta Tedeschi
Department of Electric Power Engineering
Norwegian University of Science and Technology
Trondheim, Norway
elisabetta.tedeschi@ntnu.no

***Abstract*—With an increased integration of grid-connected distributed generators in the power systems, the control structures are increasingly complex. This paper discusses a distributed energy storage technology based on battery banks. The energy storage is connected to a bidirectional DC-DC converter. The design of the battery pack and control of the converter is included in the paper. Additionally, the energy storage system is emulated with a laboratory setup through the use of a power hardware in the loop architecture. The simulations are carried out in MATLAB/Simulink and Opal-RT.**

***Index Terms*—ESS, battery system, bidirectional converter, converter control, PHiL**

I. Introduction

The electrical grid is in the midst of a significant transition. As the world's population continue to grow, more people are in need for electricity as well as the ever attention to climate change mitigation is growing. This has lead to several arising trends regarding the electricity grid. One of the clearest and most impacting of the trends is the growing use of distributed generators. When a distributed generator is connected to the distribution grid, it requires advanced control and regulation to avoid fault in system resonance and interference [1].

The technology behind DGs includes renewable energy sources (RES), non renewable electricity generators and energy storage systems (ESS). Common renewable energy sources used in distributed generation may include photovoltaic systems (PV) and wind energy systems. Distributed energy resources (DER) also include controllable loads such as plug in vehicles and power electronic loads [2], [3]. Due to the intermittent behaviour of RESs, energy storage systems play a crucial role within the power distribution in a low-voltage grid. Battery systems and hydrogen storage systems, as well as flywheels are primarily used as ESS. The implementation of ESSs supports the inertia of the grid, hence decreasing the chance of instability [4]. This is particularly important when the grid has a high degree of stochastic load penetration.

A bidirectional DC-DC converter is widely used in the ESS application, particularly in low voltage grids. The bidirectional converter connects the energy storage technology to an additional converter that links the DC side with the AC grid (see Fig. 1). An application of the energy storage system as seen in Fig. 1 requires an additional two-level voltage source converter to coordinate the power flow between the AC and DC buses. The converter's bidirectional characteristic allows for power flow both ways. This leads to an improved performance of the system as the converter allows for an efficient control of the voltage levels [5], [6].

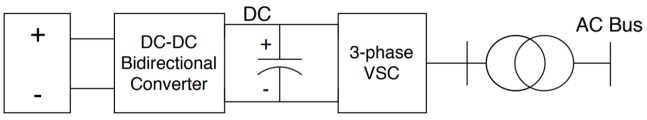

Fig. 1. Line diagram of paper scope

The paper opens with an explanation of the battery model used in the study. Further, a section on the bidirectional converter explains its behaviour and the control using Proportional - Integral (PI) regulators for voltage and current stability. Section 4 explains the Power Hardware in the Loop (PHiL) technique used to carry out laboratory testing and explains the discretization algorithm used to achieve the provided results. The computational results from implementation of the battery bank and discretized converter is given in section 5, along with the final laboratory testing results.

II. Battery System

A. Battery Model

The state of charge (SOC) of the battery can be expressed as in equation (1) [7], [8].

$$SOC = 100(1 - \frac{\int i_b dt}{Q}) \tag{1}$$

Where i_b is the battery current and Q is the battery capacity. The terminal voltage V_b is calculated as shown in (2). The open circuit voltage is expressed as V_0, the internal resistance is denoted R_b. K denotes the polarization voltage. A and B

978-1-7281-0653-3/19/$31.00 © 2019 IEEE

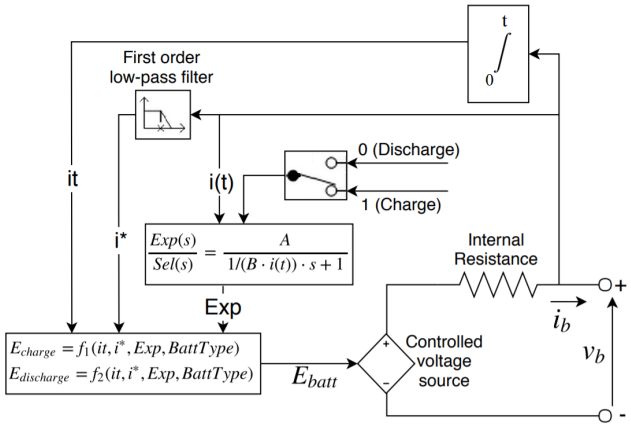

Fig. 2. Equivalent battery model from Simulink.

are the exponential zone voltage and the exponential capacity respectively.

$$E_{batt} = E_0 + R_b \cdot i_b - K\frac{Q}{Q + \int i_b dt} + A \cdot exp(-B \int i_b dt) \quad (2)$$

In the conceptual scheme in Fig. 2, E_{batt} is the nonlinear voltage. $Exp(s)$ denotes the exponential zone dynamics and $Sel(s)$ represents the battery mode, where $Sel(s) = 0$ when the battery is discharging and 1 when the battery is charging. $i*$, i_b and it are respectively the low frequency current dynamics, the battery current and the extracted capacity.
The discharge model of the Lithium-Ion battery is given in (3) and the charge model is given in (4).

$$f_1(it, i*, i) = E_0 - K \cdot \frac{Q}{Q - it} \cdot i* - K \cdot \frac{Q}{Q - it} \cdot it + A \cdot exp(-B \cdot it) \quad (3)$$

$$f_2(it, i*, i) = E_0 - K \cdot \frac{Q}{it + 0.1 \cdot Q} \cdot i* - K \cdot \frac{Q}{Q - it} \cdot it + A \cdot exp(-B \cdot it) \quad (4)$$

B. Internal resistance

The battery's internal resistance has a significant impact on the voltage drop caused by current deviation. Reference [9] discovered a mismatch between the internal resistance provided by the manufacturer's data sheet and the current variation. Therefore, a new relation was proposed as in equation (5).

$$\eta = 1 - \frac{I_{nom} \cdot R}{V_{nom}} \quad (5)$$

Where η is the efficiency coefficient. The nominal discharge curve is dependent on the rated current, I_{nom}, which therefore can be expressed as in (6).

$$I_{nom} = Q_{nom} \cdot 0.2/1hr \quad (6)$$

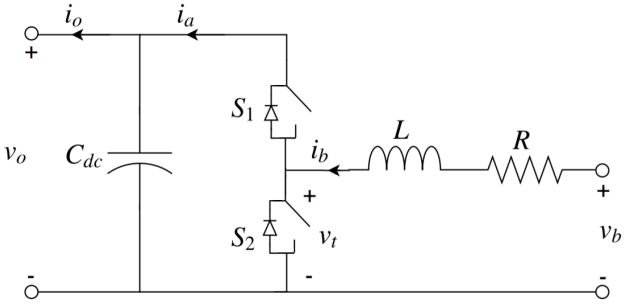

(a) Bidirectional Converter Topology.

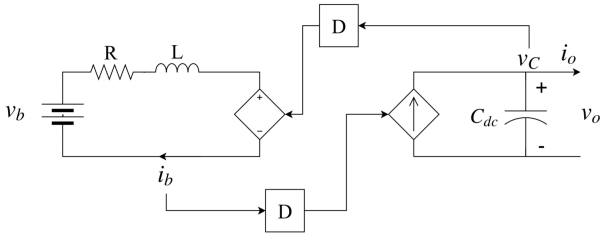

(b) Boost converter average model.

Fig. 3. Bidirectional Converter.

Substituting (5) and (6) allows the expression of the internal battery resistance as a function of the nominal voltage, the efficiency and the nominal capacity.

$$R = V_{nom} \cdot \frac{1 - \eta}{0.2 \cdot Q_{nom}} \quad (7)$$

III. Bidirectional Converter

A. Converter Behaviour

Figure 3a shows a boost converter, where the witches are operated in a complementary fashion. Hence, when the first switch, S_1 is on, the second switch, S_2, is off and vice versa. In binary form the open switch is denoted as $S = 0$ and the closed switch, when the switch is on, is denoted as $S = 1$.

B. Converter Control

1) Inner Current Control Loop: PI regulators are used in both the current and voltage control for the bidirectional converter [10]. In the boost converter topology in Fig. 3a, the battery voltage expression is:

$$v_b = Ri_b + \frac{Ldi_b}{dt} + v_t \quad (8)$$

Where v_t equals v_{out} when S_1 is closed. When S_1 is open, v_t will be 0. This gives the expression of v_t as in (9) .

$$v_t = v_o \cdot S_1 \quad (9)$$

In (8), the controlled link is $v_o S_1$, which further is expressed as μ.

$$\frac{Ldi_b}{dt} = v_b - Ri_b - \mu \quad (10)$$

The losses of Ri_b can be neglected when tuning the PI regulator.

$$K_p(i_b^* - i_b) + K_i \int_0^t (i_b^* - i_b)dt = v_b - \mu \quad (11)$$

Here, i_b^* is the reference current of the battery. The difference from the reference current to the actual current is the system error and is denoted e.

$$\mu = -(K_p e + K_i \int_0^t e dt) + v_b \tag{12}$$

Expanding μ gives a further expression of the average duty value (D). To simplify the expression, the the output voltage can be approximated at its nominal value $\overline{v_o}$:

$$D = [-(K_p e + K_i \int_0^t e dt) + v_b] \cdot \frac{1}{\overline{v_o}} \tag{13}$$

The analog sensors of the current controller is denoted as T_a and the time constant of the controller is expressed as in (14)

$$\tau = \frac{L}{\omega_b R} \tag{14}$$

Where ω_b is the base angular frequency, and L and R are the inductance and resistance, respectively. From this, the current proportional gain K_p and the current integral gain, K_i can be calculated.

$$K_p = \frac{L}{2\omega_b T_a}, \quad K_i = \frac{K_p}{\tau} \tag{15}$$

2) Outer Voltage Control Loop: Following the alternating current i_a in figure 3a, it can be observed that the current equals i_b when S_1 is on, and that the current is 0 when S_2 is off. Consequently, i_a can be expressed as:

$$i_a = i_b \cdot S_1 \tag{16}$$

The current dynamics can be written as in (17).

$$i_a - i_o = C_{dc} \frac{dv_o}{dt} \tag{17}$$

The controllable signal i_a is denoted as μ_v. Denoting the deviation between the reference voltage and v_o as the error e_v, the expression of μ_v becomes:

$$\mu_v = K_{pv} \cdot e_v + K_{iv} \int_0^t e dt + i_o \tag{18}$$

In the voltage control loop design, it is possible to use an approximation model of the current controlled loop. This approximation uses a first order model with a time constant T_e. The time constant T_e is calculated as in (19) [10].

$$T_e = 2 \cdot T_a \tag{19}$$

Where, T_a is the time constant used in the current controller for i_b described above. The proportional characteristics between i_a and i_b allows the hierarchical control strategy. The dynamic of system modelled is given in (20).

$$C_{dc} \frac{dv_o}{dt} = i_a - i_o \tag{20}$$

Where i_a is the proportional current of the inner loop as seen in figure 3a. The PI voltage controller has been tuned by applying symmetrical optimum to the per unit system inn accordance of Ref. [10].

$$K_{pv} = \frac{\omega_m \cdot C_{pu}}{\omega_b}, \quad K_{iv} = z \cdot K_{pv} \tag{21}$$

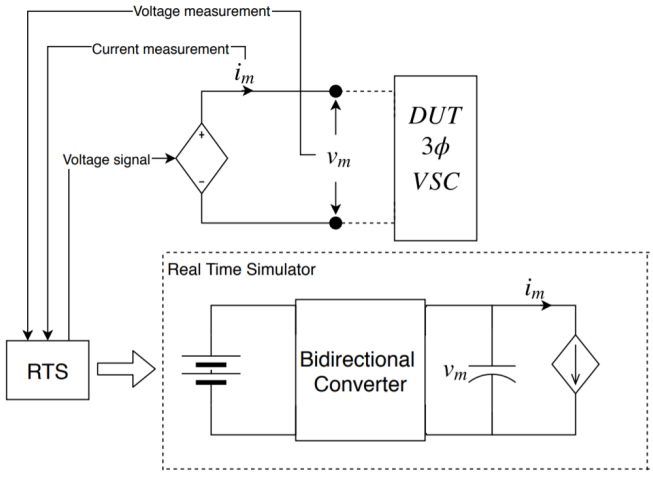

Fig. 4. Outline of PHiL Structure for emulation of ESS.

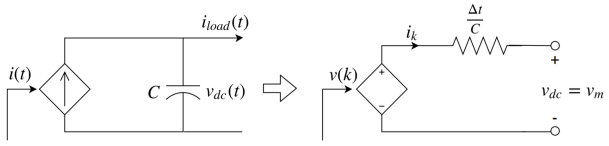

Fig. 5. Illustration of discretization objective.

IV. Power Hardware in the Loop

A. PHiL Structure

Results based on simulations have the risk of differing between different programs, mathematical models and complexity of the model. On the other hand, laboratory experiments usually comes at a high cost and requires a long developing period. Therefore, the PHiL technique is in this case used to test the system dynamics and acquire realistic results [3], [11]. The system outline is defined in Fig. 4. The converter circuit is based on an average model of the boost converter and connected to the Device Under Testing (DUT) which is a three-phase voltage source converter. From there, the measurements of voltage and current are signaled to the Real Time Simulator (RTS). The RTS simulates the energy storage model connected to the bidirectional converter and a load. As illustrated, a voltage source model is required to send the voltage reference to the controlled voltage source. In order to obtain the voltage model a discrete model at the capacitor of Fig. 4 is obtained in the following subsection

B. Discretization Algorithm

The aim of the discretization is to model the parallel connection of a current controlled source and the capacitor into its Thevenin equivalent circuit, as represented in Fig. 5. This procedure enables an emulation of the energy storage system up to the current controlled source of the high voltage side of the converter.

The Kirchhoff's current law can be described as:

$$C\frac{dv_{dc}(t)}{dt} = i(t) - i_{load}(t) \tag{22}$$

where, i(t) is controllable and $i_{load}(t)$ is the disturbance. The expression can further be represented in the Laplace domain as in (23).

$$CsV_{DC}(s) = I(s) - I_{load}(s) \tag{23}$$

where, $V_{DC}(s), i(s)$ and $i_{load}(s)$ are the same variables as above in the Laplace domain.

The trapezoidal approach of discretizing continuous signals leads to:

$$s = \frac{2(z-1)}{T(z+1)} \tag{24}$$

The system in the z-domain is represented as follows:

$$C\frac{2(z-1)}{T(z+1)}V_{dc}(z) = I(z) - I_{load}(z) \tag{25}$$

$$2C(z-1)V_{dc}(z) = T(z+1)I(z) - T(z+1)I_{load}(z) \tag{26}$$

The trapezoidal approach obtains a signal multiplied with z equals the signal one sample time ahead. This is implemented in discrete form (27) and reordered in (28).

$$v_{dc,k+1} - v_{dc,k} = \frac{T}{2C}(i_{k+1} + i_k) - \frac{T}{2C}(i_{L,k+1} + i_{L,k}) \tag{27}$$

$$v_{dc,k+1} = v_{dc,k} + \frac{T}{2C}(i_{k+1} + i_k - i_{L,k+1} - i_{L,k}) \tag{28}$$

Now using the instant time current gives the following expression in (29). (29) is used in the computational model to obtain the same signals as the continuous time model.

$$v_{dc,k} = v_{dc,k-1} + \frac{T}{2C}(i_k - i_{k-1} - i_{L,k-1} - i_{L,k}) \tag{29}$$

Finally, the circuit at the right had of Fig. 5 can be obtained from (29). Therefore, $\Delta t = \frac{T}{2}$, the voltage drop is obtained with the measured current i_k and the computed resistor $\Delta t/C$, the output voltage is $v_m = v_{dc,k}$ and the controlled voltage source is calculated with the remaining part of the terms.

V. Computational Results

A. Design of Battery

The design of the battery pack is based upon data sheet [12]. The battery system is modelled to supply a load of 15 kW for 5 hours. Consequently, the energy capacity of the ESS is 75 kWh. The output voltage v_b is modelled to 48 V and is intended to be connected to a boost converter.

Nominal voltage of one battery cell is given at 3.7 V. The output voltage is dependent on the number of battery cells connected in series. The number of batteries in series is calculated as the fraction of the total battery voltage and the voltage of one battery cell. This leads to final n_s of 13. The capacity required of battery pack is obtained from the system load and output voltage, which gives a capacity of 1559.25 Ah. The capacity per cell is given as 2.6 Ah. The capacity of the battery pack is dependent on the number of batteries in parallel.

$$n_p = \frac{1559.25}{2.6} = 599.71 \approx 600 \tag{30}$$

TABLE I
Battery Block Parameters

Parameter	Value
Nominal Voltage (V)	48.1
Rated Capacity (Ah)	1559.25
Cut-off Voltage (V)	39
Fully Charged Voltage (V)	54.6
Nominal Discharge Current (A)	312
Internal Resistance (Ohms)	0.0154
Capacity at Nominal Voltage (Ah)	1560
Exponential Zone Voltage (V)	51.86
Exponential Zone Capacity (Ah)	76.61

The battery efficiency coefficient of a lithium-ion battery is typically $80\ -90\%$ [13]. It is assumed that the battery pack holds an efficiency of 90%. The internal impedance given in the data sheet is set to $\leqslant 180$ mΩ. However, considering section II-B, the internal impedance will be calculated according to (7), resulting in R = $0.0154\ \Omega$.

B. Energy Storage Implementation in Simulink

All the retrieved values are collected in table I and implemented in the Simulink battery model. The data regarding voltages were retrieved from the data sheet and multiplied with n_s, while the capacity and current values were multiplied with n_p as described above.

Figure 6 illustrates the nominal discharge characteristic curve of the battery using the model values from Table I. The nominal discharge current is set at $312A$. The exponential voltage drop when the battery is charged is represented by the yellow section of the graph. This section lasts from $t = 0$ to $t = 0.23$ which is at 13.8 minutes. The second zone is the area in where the charge can be extracted from the battery until the voltage is below the nominal voltage. The nominal voltage is here set to the default value of $7.2V$. After this, the voltage drops rapidly and this section represents the total discharge of the battery at 5 hours.

C. Discretization of Converter

To ensure realistic simulation results in view of the experimental validation, noise was added to the computational model in the output voltage and current. The variance of the noise is attained from tests at the Norwegian Smart Grid Laboratory. Voltage variance is set to 0.1150 and current variance is set to 0.0609. The model setup of the energy storage system has a low capacitance from design. Besides, the capacitor in the physical converter at the laboratory has a value of $14mF$ which is larger. Additionally, the current step from 1

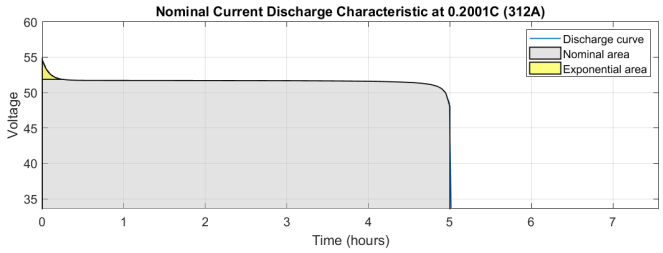

Fig. 6. The nominal discharge curve of the battery.

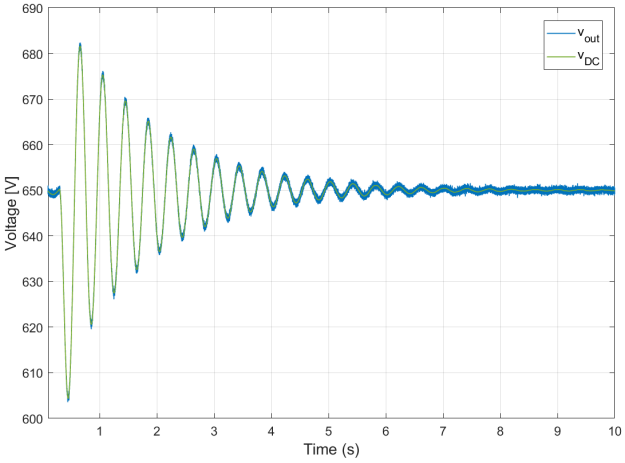

Fig. 7. Voltage output V_{out} from the continuous model and v_{DC} from the discrete model.

to 12 amperes is relatively big. This causes a slow response which leads to large and low frequency oscillation in both the voltages and currents. Figure 7 shows that the voltages of the continuous and discretized model behave similarly, with the initial oscillation before both stabilize at the desired output voltage of $650V$. The currents in Fig. 8 also show corresponding performance with the added noise.

D. Laboratory Implementation

The laboratory testing was conducted in the Norwegian Smart Grid Laboratory (see Fig. 9). The model was implemented with an OPAL - RT simulator with a sampling time $Ts = 100\mu$s, which signalled the physical laboratory equipment. The following results in Fig. 10 and 11 are obtained from a closed loop test at three different sections from logging. The blue section represents an initial steady state operation before the current is gradually increased, which also increases the amplitude of the voltage noise. The green section shows a further increase in current, while the orange section represents the section of fast decrease which gives the largest impact on the voltage. The dashed gray line between the logged signals are the estimated average value of respectively voltages and currents. Figure 10 depicts the voltage graph with an average voltage level of $650V$. Figure 11 shows the current i_k from

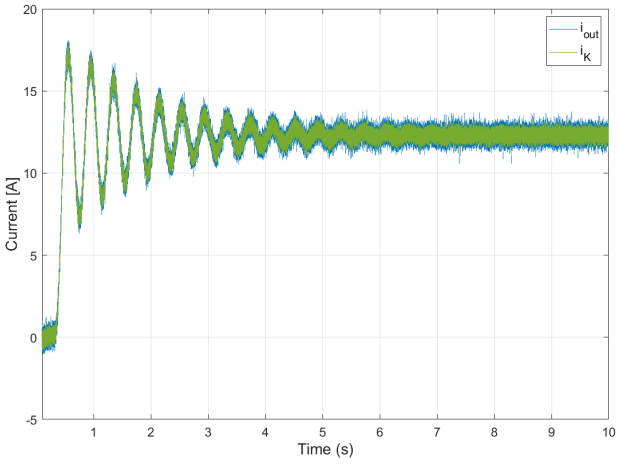

Fig. 8. Current output i_{out} from the continuous model and i_K from the discrete model.

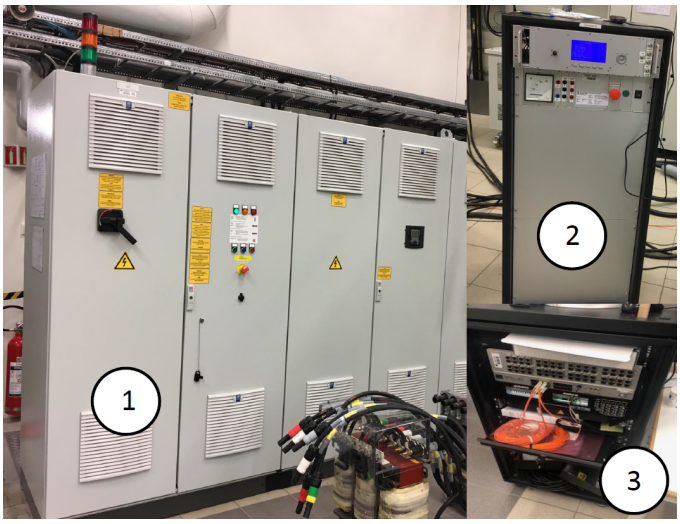

Fig. 9. Norwegian Smart grid Laboratory. (1): 200kVA Controlled Voltage Source, (2): 60 kVA $3-\phi$ VSC, (3): OPAL-RT.

the physical measurement as the black line which is always within the continuous model current i_{out}.

VI. Concluding Remarks

This paper discusses an energy storage emulation for the application of low voltage grid connection. A battery modelled is described theoretically and designed to meet set requirements. The ESS is simulated in the MATLAB/Simulink environment, which illustrated that the battery pack complied with the requirements. A bidirectional DC-DC converter is connected to the energy storage pack. The converter behaviour is explained, as well as an included part about converter control based on an average model. The voltage and current control was based on PI regulation to ensure system stability. Preceding the laboratory testing, the PHiL technique was implemented to acquire realistic results. In order to obtain the voltage model

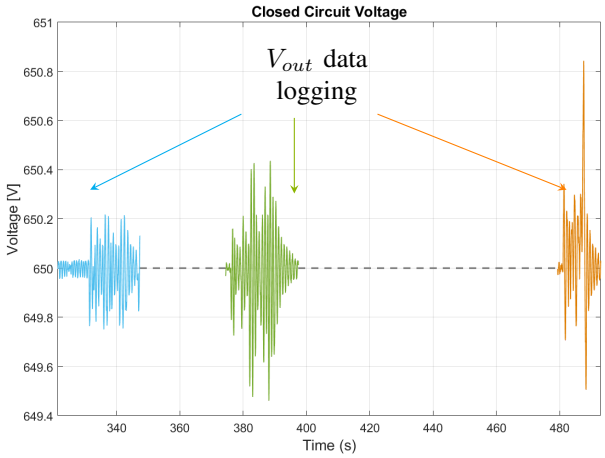

Fig. 10. Voltage output V_{out} from the continuous model and v_{DC} logged from the physical equipment perfectly correlated. Blue: first storing data in ramp test. Green: second storing data in ramp test. Orange: Third storing data current decreasing ramp. The gray dashed line represents a constant estimated average between data loggings.

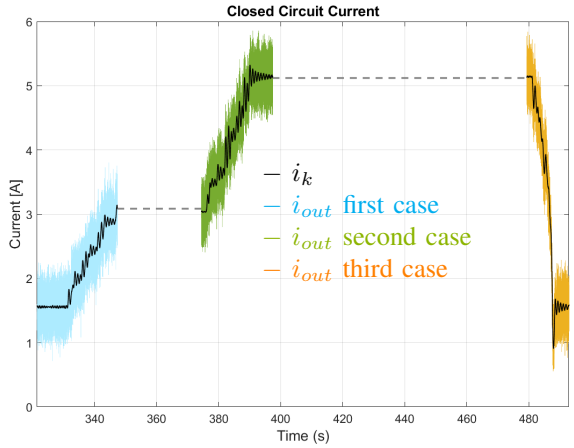

Fig. 11. Current output i_{out} from the continuous model and i_K i_k from the physical measurement as the black line. Blue: first storing data in ramp test. Green: second storing data in ramp test. Orange: Third storing data current decreasing ramp. The gray dashed line represents a constant estimated average between data loggings.

for the PHiL setup, a discrete model was derived theoretically before it was tested through simulation. The computational results presented acceptable outputs. The laboratory implementation was conducted and presented an identical voltage behaviour in the simulated and physical measurements. The current results were also achieved according to the desired output. The notable noise in the current graph is the result of using sensors rated to much higher currents, leading to a sensitive low current operation.

REFERENCES

[1] E. Pritchard, L. Mackey, D. Zhu, D. Gregory, and G. Norris, "Modular electric generator rapid deployment dc microgrid," *2017 IEEE Second International Conference on DC Microgrids*, pp. 106–110, 2017.

[2] Nwulu, N. I., and X. Xia, "Optimal dispatch for a microgrid incorporating renewables and demand response," *Renewable Energy*, vol. 101, pp. 16–28, 2017.

[3] W. Zaixing, F. Fei, L. J. Seng, S. K. Yak, X. Liu, M. A. Zagrodnik, and A. K. Gupta, "Reduction of common mode voltage of 2-level voltage source inverter-fed machine," in *2017 Asian Conference on Energy, Power and Transportation Electrification (ACEPT)*, 2017, pp. 1–5.

[4] F. A. Inthamoussou, J. Pegueroles-Queralt, and F. D. Bianchi, "Control of a supercapacitor energy storage system for microgrid applications," *IEEE Transactions on Energy Conversion*, vol. 28, no. 3, pp. 690–697, 2013.

[5] L. Ni, D. J. Patterson, and J. L. Hudgins, "High power current sensorless bidirectional 16-phase interleaved dc-dc converter for hybrid vehicle application," *IEEE Transactions on Power Electronics*, vol. 27, no. 3, pp. 1141–1151, March 2012.

[6] X. Li, W. Zhang, H. Li, R. Xie, and D. Xu, "Design and control of bi-directional dc/dc converter for 30kw fuel cell power system," in *8th International Conference on Power Electronics - ECCE Asia*, May 2011, pp. 1024–1030.

[7] X. Liu, P. Wang, and P. C. Loh, "A hybrid ac/dc microgrid and its coordination control," *IEEE Transactions on Smart Grid*, vol. 2, no. 2, pp. 278–286, June 2011.

[8] S. Sanchez, M. Molinas, M. Degano, and P. Zanchetta, "Stability evaluation of a dc micro-grid and future interconnection toan ac system," *Renewable Energy*, vol. 62, pp. 649 – 656, 2014. [Online]. Available: http://www.sciencedirect.com/science/article/pii/S096014811300428X

[9] O. Tremblay, L. Dessaint, and A. Dekkiche, "A generic battery model for the dynamic simulation of hybrid electric vehicles," in *2007 IEEE Vehicle Power and Propulsion Conference*, Sep. 2007, pp. 284–289.

[10] S. Sanchez, G. Bergna, and E. Tedeschi, "Tuning of control loops for grid-connected modular multilevel converters under a simplified port representation for large system studies," in *2017 Twelfth International Conference on Ecological Vehicles and Renewable Energies (EVER)*, April 2017, pp. 1–8.

[11] S. Sanchez, S. D'Arco, A. Holdyk, and E. Tedeschi, "An approach for small scale power hardware in the loop emulation of hvdc cables," in *2018 Thirteenth International Conference on Ecological Vehicles and Renewable Energies (EVER)*, April 2018, pp. 1–8.

[12] *Lithium-Ion Battery*, EEMB Co., Ltd, 8 2016.

[13] L. Valen and M. I Shoesmith, "The effect of phev and hev duty cycles on battery and battery pack performance," 03 2019.